Global NEST Journal, Vol 25, No 6, pp 109-118

Valorization of *Annona reticulata* biochar by chitosan for the adsorption of azo dye from textile effluent

Rajakumar S.[1,*], Ramakrishnan.S.[2], Monica Nandini G.K.[3], El-marghany A.[4], Warad I.[5,6]. and Kumar M.S.[7]
[1]Department of Civil Engineering, University VOC College of Engineering, Anna University Thoothukudi Campus, Thoothukudi – 628 008, Tamil Nadu, India.
[2]Department of Civil Engineering, Sri Krishna College of Engineering and Technology, Coimbatore – 641 008, Tamil Nadu, India
[3]Department of Civil Engineering, Sona College of Technology, Salem – 636 005, Tamilnadu, India
[4]Department of Chemistry, College of Science, King Saud University, P.O. Box 2455, Riyadh 11451, Saudi Arabia
[5]Department of Chemistry, AN- Najah National University, P.O. Box 7, Nablus, Palestine
[6]Research Centre, Manchester Salt & Catalysis, Unit C, 88-90 Chorlton Rd, M15 4AN Manchester, United Kingdom
[7]Department of Environmental Engineering, College of Engineering and Technology, Bule Hora University, Bule Hora, West Guji, Ethiopia
Received: 14/03/2023, Accepted: 12/04/2023, Available online: 18/04/2023
*to whom all correspondence should be addressed: e-mail: civilrajas@gmail.com
https://doi.org/10.30955/gnj.004882

Graphical abstract

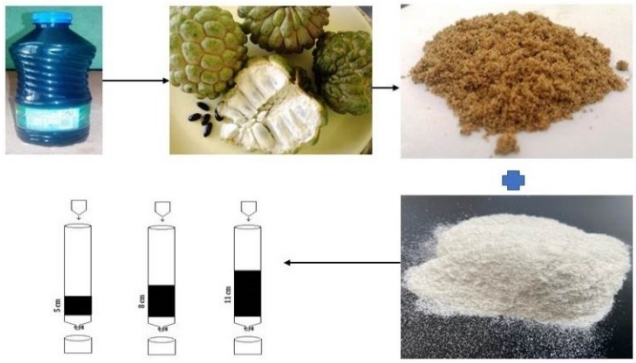

Abstract

Azo dye is a synthetic aromatic dye which are direct dye frequently used in textile industry to colour fibres. It also contributes to the damage of the environment. This study examines the adsorption biochar made from Annona reticulata to remove azo dye from textile wastewater. To improve the adsorption capacity, biochar valorized by chitosan molecules, Investigations were conducted on the use of chitosan-based materials that are acid-resistant for azo dye adsorption. In the batch experiment, basic operating parameters such as initial Azo dye concentrations, pH, contact time and bed height were assessed. The percentage removal efficiency for Azo dye was recorded as 67.18%, 75.88% and 94.37% for three dissimilar sized columns that were 6cm, 8cm, and 10cm. The UV–visible absorption spectroscopy was used to quantify the decolorization of dyes. The changed surface properties of the adsorbent produced from Annona reticulata were characterized by using SEM, XRD, and FTIR. The effectiveness of the column's adsorption was calculated mathematically by Yoon-Nelson, Thomas, and Adams-Bohart models. The model that best represents equilibrium isotherm data by adsorption had R^2 values of 94.63, 86.67 and 96.35 respectively.

Keywords: Azo dye removal, textile wastewater, annona reticulata, chitosan, adsorption

1. Introduction

The textile industry is one of the major contributors to serious pollution issues around the world because it is a significant industrial consumer of water and a significant producer of wastewater (Kamboh *et al.*, 2014). The increased demand for textile products has also led to an increase in the generation of textile wastewater (Krishnakumar *et al.*, 2014). The classification of textile industries is based on the kinds of fabrics they create, such as cellulosic materials derived from plants, protein fabrics derived from animals, and synthetic fabrics created artificially (Gokulan *et al.*, 2022). In textile factories, both dry and wet techniques are used to produce fiber. The wet procedure releases highly contaminated wastewater while using a sizable amount of potable water (Sujatha *et al.*, 2022). This procedure includes techniques for sourcing, sizing, de-sizing, bleaching, mercerizing, dyeing, printing, and finishing. The discharged colored effluents are a significant non-aesthetic pollution source, and the oxidation, hydrolysis, or other chemical reactions that occur during the wastewater phase result in hazardous by-products that are released into the environment (Gokulan *et al.*, 2022). The textile industry's primary environmental harm comes from the discharge of untreated effluents into water bodies, which typically account for 80% of all emissions produced by this sector (Praveen *et al.*, 2021). Biochemical oxygen demand (BOD) and Chemical oxygen demand (COD) are relatively high levels in most residual fluids from the textile industry (Ravindiran *et al.*, 2019). The abundance of non-biodegradable chemical substances,

particularly textile colors, should receive more attention (Rao *et al.*, 2021). Azo dye molecules are harmful to higher living organisms, including aquatic environments and plants, since they are toxic, carcinogenic, teratogenic, and mutagenic. Approximately 15-20% of azo dyes are discharged as wastewater into aquatic habitats because they are not anchored to the substrate (Gokulan *et al.*, 2021). A serious threat to aquatic life and indirectly to human health is posed by the presence of minute amounts of azo dyes, which are quite apparent and have a negative impact on the clarity and quality of water bodies like lakes, ponds, and rivers (Sujatha*et al.*, 2021). Bladder cancer in humans has been connected to azo dye ingredients like benzidine. Moreover, azo dye exposure increases the risk of bladder cancer in dye workers (Gokulan *et al.*, 2019). Therefore, azo dyes are genotoxic, mutagenic, carcinogenic, and have deadly consequences on both people and animals. The reckless release of azo dyes into the environment, especially from the textile industry, is of great concern to both human health and the environment (Kalyani *et al.*, 2021). One of the unit activities in the chemical engineering procedures used to treat the wastewater from the textile industry is adsorption (Ravindiran *et al.*, 2019). Due to the ease of the procedure and reduced cost compared to other processes, adsorption is a well-established technology for azo dye removal from wastewater (Madhu *et al.*, 2021). The technique becomes even more economically efficient when adsorbents made from different biomass wastes, such as biochar and activated carbon, are developed (Gokulan *et al.*, 2019). For the treatment of dye wastewater, biochar has been found as a possible contender. Due to the presence of surface functional groups and the biochar's substantial surface area, it is advantageous to employ biochar for wastewater treatment (Priya *et al.*, 2020). Several studies have investigated the environmentally beneficial usage of biochar for the removal of colour from textile effluent in the past (Gokulan *et al.*, 2019). The purpose of this study was to investigate how effectively azo dye might be removed from treated textile effluent (Mahendran *et al.*, 2021). Batch adsorption process was proceeded for the removal of azo dye and UV–visible absorption spectroscopy was used to quantify the decolorization of dyes (Gokulan *et al.*, 2020). SEM, XRD, and FTIR characterisation techniques provided strong support for the experiment. The mathematical modelling Yoon-Nelson, Thomas, and Adams-Bohart models were reinforced the adsorption process (Murugadoss *et al.*, 2021). Intraparticle diffusion model and repeated studies of the adsorbent's regeneration capacity was conducted.

2. Martials and methods

2.1. Preparation of column material

The Annona reticulata seed was collected, dried completely for 10 hours at 100°C in a hot air oven, and then manually broken into numerous pieces (Gokulan *et al.*, 2021). The microbiological particles were fully crushed out after that, and the column material was collected and cleaned with a NaCl solution (Kumar *et al.*, 2021). Again, it was allowed to dry for 10 hours in a hot air oven set to 100°C and for 5 hours in the open air.

2.2. The adsorbent surface activation by chitosan particles

100 mL of a 0.1M acetic acid solution were used to dissolve 0.5 g of chitosan to create the basic chitosan solution (Gokulan *et al.*, 2021). The dissolution process took place at room temperature for 3 hours with constant stirring, after which the solution was left to stand for 10 hours (Sundar *et al.*, 2021). Sulfate anions were used as crosslinking bridges to create chitosan nanoparticles. By combining a solution of chitosan with a solution of K2SO47H2O at a constant concentration in a volume ratio of 1:1 while stirring (Gokulan *et al.*, 2022), chitosan sulfate aqueous dispersions were created. Chitosan was present in the combinations at a constant concentration of 2 gL^{-1} (Jegan *et al.*, 2020). SEM surface examination of a superficially modified adsorbent.

2.3. Column study

The particle sizes ranging from 0.8 mm to 3 mm of adsorbent was prepared and it was filled in column and the bottom was covered with class glass wool (Praveen *et al.*, 2021). The three different sized 6cm, 8cm and 10cm filled adsorbent column with the flow rate of 3 ml/min was used for the adsorption study (Sujatha *et al.*, 2021). The column study conducted in the room temperature, In the fixed bed column studies, a glass column with an inner diameter of 3 cm and a length of 80 cm was used (Pushpa *et al.*, 2019).

2.4. Spectrophotometric analysis

HCl or NaOH solutions were used to modify the pH of the solution. In each experiment, which was carried out twice (Senthil Kumar *et al.*, 2021) The UV-visible spectrophotometer method was used to determine the amount of dye in the solutions. With the following expression, the amount of dye adsorbed per unit mass of resin was determined:

$$q_e = (C_0 - C_e)\, x\, V / (m)$$

Where Co and Ce (mg/L) were the preliminary and symmetry dye concentrations in the aqueous solution, and the adsorbent capacity, qe (mg/g) (Hariharan *et al.*, 2022); The experimental solution's volume, V (ml), and adsorbent's weight, m (g), were both given.

2.5. Kinetic study

2.5.1. Thomas model

The Thomas model was used to calculate the relationship between solute concentration and time (Jegan *et al.*, 2021). In continuous column technology, both internal and external mass transfer restrictions were considered.

$$\mathrm{Ln}\left(\frac{Co}{Ct} - 1\right) = (\mathrm{Kt} * q * m / Q) - kt * Co * t$$

where m is the mass of the adsorbent, Co and Ct are the influent and effluent concentrations (mg/L), Kt is the Thomas rate constant (mL/(min.mg), and t is the duration (min), Assuming a constant flow rate, the volume of adsorbent in the column was restrained as Q (g), and the

adsorption kinetics (kt) were determined from the plot of ln [(co/ct)] over time (Praveen *et al.*, 2022).

2.5.2. Adams-Bohart model

Construction of fixed bed columns most usually employs the Adams Bohart. This model was developed with the presumption that the adsorbate is quickly adsorbed onto the adsorbent surface, and that intra-particle diffusion and external mass transfer resistance are unimportant factors (Kumar *et al.*, 2022). The first 10 to 50% of the saturation points, or the breakpoint, of the breakthrough curve, are identified using this model.

$$R_e = \ln\left(\frac{Ct}{Co}\right) = Kab\ Cot - Kab\ Nab\left(\frac{z}{u}\right)$$

The kinetic constant in this equation is represented by kab (L/mg min), the linear flow velocity is denoted by u (cm/min), and the saturation concentration is designated by Nab (mg/L) (Jegan *et al.*, 2020). The parameter values for kab and Nab were obtained by plotting the function ln (Ct/C0) versus t and calculating its slope and intercept. The kinetic constant kab changed as the inlet flow rate and initial dye concentration increased and decreased, respectively (Ragunath *et al.*, 2022). Nab's value increased with increasing starting concentrations. In the start of the adsorption process, external diffusion can be the reason for this. The statistic that some data did not appropriate the model precisely confirmed its errors.

2.6. Characterization of adsorbent

2.6.1. SEM analysis

Adsorption images were captured using the SEM analytical technique. Using geometrical information from two-dimensional photos, the estimation of flocculation and aperture properties of surface area was carried out utilizing image dispensation software (Saravanan *et al.*, 2022). Examining was done using scanning electron microscopes (SEM), specifically an APE-60 syrmaks R-560 SEM equipped with 800 EDS spectrometer and an HDP-EDS detector, in order to confirm the deposited sludge during the flocculation process (Ilavarasan *et al.*, 2022). The execution of all extent on elegant segments was made possible by acerbating the samples and rasping the saturated segments (Gokulan *et al.*, 2020). To assess any compositional adjustment based on the intricate array of different capabilities present within the cohort of the analytical signals (Praveen *et al.*, 2021). For the experiments to generate data that was at least passably illustrative, 800x magnification was used. This resembles squares about 1 mm2 in size (Ravindiran *et al.*, 2014). In both configurations, the analyses were carried out by searching four areas for each taster.

2.6.2. XRD analysis

Azo dye removal in aqueous solution as determined by adsorption research. Highest expected dense resolution for the main Azo dye constituents, as shown by XRD (Kumar *et al.*, 2017). Using a tube driven by X-ray diffraction, measurements of the overall concentration of the major and minor components in the adsorption were made (XRD) (Gokulan *et al.*, 2018). The operational parameters of the Topins X-ray apparatus model SNLH0 were 0 kV and with 6000 seconds were spent irradiating (Krishna *et al.*, 2015). A Si (Li) detector was used to create the X-ray spectra, which were then analysed using the reiterative smallest quadrangular accurate computer code. IFEA standard orientation material analyses were finished as part of the measurement quality control process (Gokulan *et al.*, 2013). The stream cell contains an adsorbent sample with electrochemical responses and diffraction patterns that have been recorded (Rajeshkumar *et al.*, 2023). The in situ electrochemical dimension that the arrangement supports is its key strength. The deflection patterns are made possible by the moving brine (Gokulan *et al.*, 2014). Since it took that long to complete the security checks and depart the experimental hutch, the XRD measurements began 6–10 minutes after the flow began through the cell.

2.6.3. FTIR analysis

Using a Spectrum Two-Perkin Elmer Model, Fourier transform infrared spectroscopy (FTIR) was used to see the actual clusters in molecular structures at ambient temperature. The IR spectra were used to monitor the actual assembly (DadbanShahamat *et al.*, 2022). The vibration of the band at 640 cm^{-1} is associated with (AlCl). Due to different surroundings, (Al-O's) vibration appeared in two distinct frequencies (Al-O) (Ravindiran *et al.*, 2014). As a result, the peak at 1536 cm^{-1} is like the NaCl bond expanding. Stretching and bending of the bands seen at 1742 cm^{-1} and 2610 cm^{-1} are attributed to (OH). The vibration of the band at 4254cm^{-1} is (Al-OH) (Moradi *et al.*, 2022). These allotted objects make up the adsorbent stages (Ravindiran *et al.*, 2014). As they provide a variety of important information, the characteristic peaks of the amide groups band in FTIR are helpful for analyzing the structure of the deposited sludge (Gao *et al.*, 2013). The FTIR spectra of various temperature-treated adsorbents were displayed. 60 minutes were spent treating the samples at various temperatures (Xi *et al.*, 2013). From discs containing adsorbent-deposited sludge samples, FTIR spectra were obtained (Hashemi *et al.*, 2022). Using an infrared spectrophotometer, the spectra were measured from 6000 to 600 cm^{-1} at a data acquisition rate of 6 cm^{-1} per point.

2.6.4. Study on intraparticle diffusion

It was done using the Weber-Morris intraparticle diffusion model (Zubair *et al.*, 2022). The subsequent equation assisted as the primer to this study:

$$q_t = K_{id} t^{0.5} + C$$

K_{id} is the rate constant of the intraparticle diffusion model, and C is a constant (mgr/gr). The linear relationship between the values of qt and t is 0.5 can be used to derive the values of Kid and C.

2.7. Regeneration of adsorbent

By electrically heating the adsorbent to 400°C in both an inert and an environment with air, thermal regeneration was accomplished (Amani-Ghadim *et al.*, 2013). The adsorbent was heated to 400°C to 600°C in a muffle furnace during the hot water extraction process, twice washed with

DI water and HCL solution, and then dried for an additional three hours in a hot air oven (Ozdemir *et al.*, 2013). The effectiveness of the regenerated adsorbent's regeneration was determined by evaluating the azo dye removal capacity.

3. Result and discussion

3.1. Adsorption study

Azo dye was primarily existing in effluent at a meditation of 270 mg/L. Batch process research performed to examine Azo dye adsorption in order to evaluate how well Annona reticulata - chitosan assisted as an adsorbent for the elimination of Azo dye (Patel *et al.*, 2013). In order to gauge how well the treatment was functioning, samples were obtained every 10 minutes and analyzed using a UV-visible spectrophotometer technique. Studies on the initial investigation using Annona reticulata-chitosan columns were done (Hua *et al.*, 2013). Although the input trial level was 3 mL/min in a 6 cm stake, the output ranges were 1.6 mL/min. According to Table.1 & Figure 1, In 80 minutes, the column was totally drained at 88.6 mg/l for 6 cm.

Table 1 Azo dye removal for 6cm column

Time (min)	6cm column (mg/L)
0	270.0
10	213.4
20	198.7
30	175.6
40	167.5
50	133.9
60	116.3
70	108.7
80	88.6
90	88.6

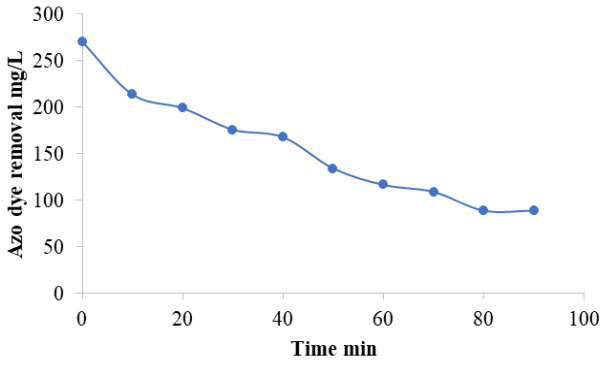

Figure 1. Azo dye removal for 6cm column

The elimination percentage in the initial adsorption study reached about 67.40%. On the second round of the study, investigations were done using Annona reticulata-chitosan columns (Morshedi *et al.*, 2013). The output ranges were 1.2 mL/min, while the input sample flow rate of 3 mL/min in an 8 cm column was kept constant (Wang *et al.*, 2013). According to Table 2 and Figure 2, Within 110 minutes, the column was entirely drained at 65.1 mg/l for 8 cm.

Table 2 Azo dye removal for 8cm column

Time (min)	8cm column (mg/L)
0	270.0
10	258.3
20	192.6
30	185.3
40	177.9
50	153.5
60	133.7
70	118.9
80	90.5
90	85.6
100	78.3
110	65.1
120	65.1

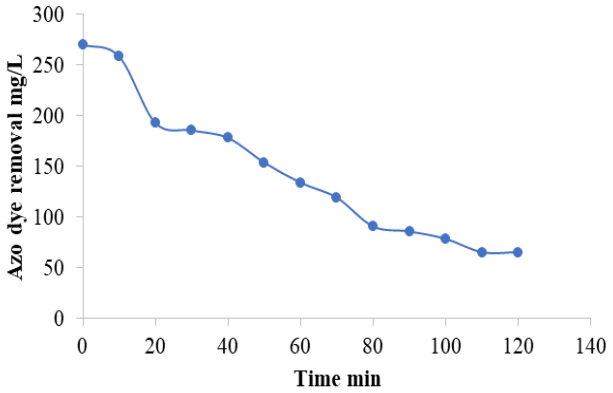

Figure 2. Azo dye removal for 8cm column

The elimination percentage reached about 75.88% in the second round of the adsorption investigation (Al-Amrani *et al.*, 2014). Studies were done employing Annona reticulata-chitosan columns during the third round of the investigation. The output ranges were 1 mL/min, while the input sample flow rate was maintained at 3 mL/min in a 10 cm column (Zhang *et al.*, 2014). According to Table 3 and Figure 3, the column was completely depleted at a rate of 15.2 mg/l for 10 cm in 120 minutes, with a removal percentage of 94.37%.

Table 3 Azo dye removal for 10cm column

Time (min)	10cm column (mg/L)
0	270.0
10	218.5
20	164.8
30	127.6
40	103.5
50	92.4
60	76.5
70	54.2
80	38.7
90	27.9
100	16.5
110	15.8
120	15.2
130	15.2

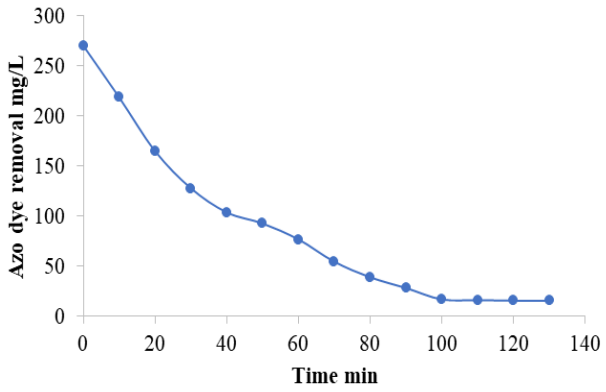

Figure 3. Azo dye removal for 10cm column

In the extensive column experiment, the initial azo dye concentration in the effluent was 270 mg/L. Using batch process study, it was feasible to assess how successfully Annona reticulata - chitosan removed Azo dye when used as an adsorbent (Tuttolomondo *et al.*, 2014). The output ranges for the three different sized columns 6, 8, and 10 cm differ according to the height of the bed. For the 6cm column, the output ranges were 1.6 mL/min, for the 8cm column, 1.2 mL/min, and for the 10cm column, 1 mL/min, due the height of bed the infiltration ranges vary (Shirzad-Siboni *et al.*, 2014). To gauge how much of the azo dye had been removed from the sample, a UV-visible spectrophotometer was employed.In this study, the removal range for a 6 cm column was 88.6 mg/L, and after 80 minutes, the adsorption column reached saturation with a removal percentage of roughly 67.40%. The azo dye removal range in the following investigation for an 8 cm column was 65.1 mg/L in 110 min, and the adsorption column was saturated with a removal percentage of roughly 75.88%. The end experiment had a height of 10 cm, a removal range of 15.2mg/L in 120 minutes, and a removal percentage of 94.37% (Li *et al.*, 2022). This study demonstrated how the elimination of azo dye is influenced by the contact time, flow velocity, and column depth. The size of the column was determined at 6 cm, 8 cm, and 10 cm based on the thorough study. The column separates the azo dye from the wastewater because of its infiltration capability (Gnanasekaran *et al.*, 2022). This experiment used a surface-modified adsorbent to regulate the ideal azo dye concentration in the textile effluent.

3.2. Kinetic study

3.2.1. Adsorption experiment analysed by Thomson model

The ionic speciation of the adsorbate laid in the required region controlled the adsorption process. It was assessed using the Thomas model (Kalyani *et al.*, 2020). The measured and predicted break-through curve for the adsorption process agreed, as evidenced by the maximum regression coefficient value (R^2) for a 10 cm column, which was 0.972. The greatest concentration of adsorbate had favorable adsorption kinetics, as evidenced by the mass (m) and time of concentration effect kt's value (t) (Jegan *et al.*, 2020). Kt values initially minor, and in subsequent stage it increased as 0.027, 0.024, and 0.029 for the column. Temperature increase caused a decrease in the rate constant (kt). The equilibrium uptake capacity slightly increased (qo). The decrease in qo showed that, as the chart plainly states, the adsorption capacity is negatively associated with bed height and contact time.

3.2.2. Adams-Bohart model

The 60% of the saturation points of the breakthrough curve are described by this model. The kinetic constant Kab varied as the initial adsorbent concentration, bed height, and inflow flow rate did, in that order (Jankowska *et al.*, 2022). Nab's value is developed at higher original solvent concentrations. This may have occurred at the beginning of the electro adsorption process due to diffusion from the outside. Tables 4 and 5 exhibits the standard for R^2, Kab, and Nab. As not all values fit into the model, it had limits.

Table 4 Adsorption experiment analysed by Thomson model

Material	Column size (cm)	k_t x 10^{-3} (mL/(min.mg)	q_o (mg/g)	R^2
Annona reticulata	6	0.027	6.52	0.901
Chitosan	8	0.024	3.40	0.936
	10	0.029	6.86	0.972

Table 5 Adams-Bohart model for Three different study

Material	Column size (cm)	N_{ab} (mg/L)	K_{ab} (ml/mg min)	R^2
Annona reticulata	6	146.10	0.0017	0.913
Chitosan	8	137.41	0.0028	0.948
	10	187.22	0.0032	0.975

3.3. Characterisation study

3.3.1. SEM analysis

SEM pictures were used to describe the microstructures and morphologies of Annona reticulata - Chitosan. Figure 4 illustrates how the dark-colored structural modifications and abundant asymmetrical shacks in azo dye result in more lively adsorption sites (Lach *et al.*, 2022). A closer look at the structure revealed that it had retained its black color long after magnetization. With a diameter of about 350 nm, the crystal domains are consistently ornamented and decisively attached to the adsorbent surface in accordance with the magnetic microspheres created adsorbent surface changes (Gungor *et al.*, 2008). As shown in Figure 4 with varying sizes presenting a block-like structure and smooth surface, for compelling separation, a homogeneous distribution of magnetite on the adsorbent's external is beneficial.

Figure 4. SEM analysis of Annona reticulata – Chitosan adsorbent

3.3.2. XRD analysis

Figure 6 displays the XRD patterns of the Annona reticulata-Chitosan adsorbent. The diffusion pattern of the adsorbent lacks a glassy peak, indicating an amorphous structure for the azo dye adsorption (Murali *et al.*, 2013). Figure 5 illustrates how XRD reveals the distinctive peaks of an adsorbent at 40.5 ° (250), 36.3 ° (352), 42.5 ° (280), 58.7 ° (613), and 69.5 ° (540). The outcomes imply that the introduction of the magnetic adsorbent into the adsorption study was successful. Also, unlike the XRD patterns of azo dye removal, no carbon peak was seen for the adsorbent, showing that it still has an amorphous structure following hydrothermal magnetization (Pushpa *et al.*, 2021). They exhibit a type I isotherm now, which suggests that they are mesoporous. This is added reinforced by its minute hysteresis rings in the relative pressure P/P0 region between 0.2 and 0.6. According to their pore structure properties, azo dye has a lower surface area and pore volume (2653 m2 and 1.53 cm3, respectively) while adsorbing than adsorbent (3261 m2 and 1.84 cm3, respectively). Because mutually high and low external area carbonaceous elements are used to create the magnetic composite, the exact adsorbent's superficial area was decreased (Figure 5).

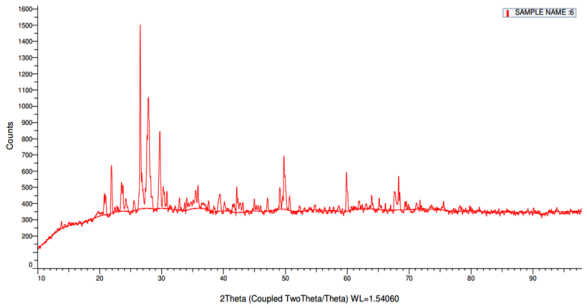

Figure 5 XRD analysis of Annona reticulata – Chitosan adsorbent

3.3.3. FTIR analysis

Figure 6 shows the FTIR spectrum of the Annona reticulata-Chitosan adsorbent. There are some adsorbed azo dyes and coordinated water present at the same time, as shown by the faint absorption peaks at 3421 and 453.27 /cm, which pertain to the circuitous trembling and stretching vibration of the OH- bond (Vucurovic *et al.*, 2014). In the case of an adsorbent, A peak at 2883.58 cm was found by XRD examination, and it may be associated to the flexural vibration of C-H, as well as bands at 2831.50 cm and 2385.95 cm that were ascribed to the O-H distortion trembling and the C=C extending quivering (Haris *et al.*, 2022). The large absorption maxima at 1633.71 cm and 727.16 cm of Annona reticulata-Chitosan adsorbent are attributed to the carboxyl groups' (-C=O-) and C-H bending vibrations. C-O stretching and O-H bending (in-plane) vibrations are responsible for the broad band that may be seen between 1043.49 and 775.38 cm.

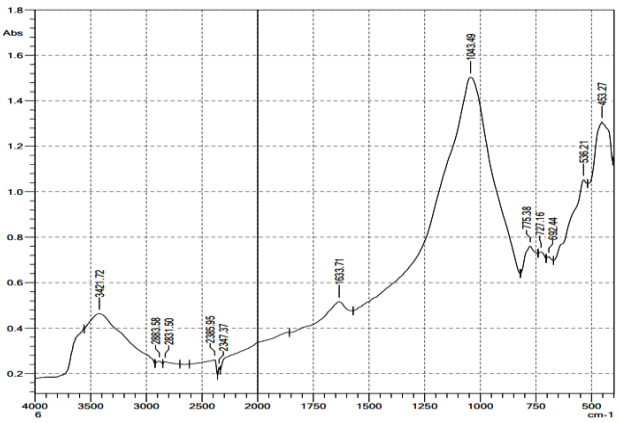

Figure 6 FTIR analysis of Annona reticulata – Chitosan adsorbent

3.4. Intra particle diffusion model

High regression coefficient (94%–96%) from experimental model constructed and reported in Table 6, it is believed that this kinetic model provides the most accurate description of the adsorption of Annona reticulata–chitosan isomers. Azo dye demonstrated a higher removal rate and adsorption loading compared to other isomers (Xu *et al.*, 2014). In some situations, the presence of methyl groups may speed up clearance. The intraparticle diffusion study shown in Table 6 are not adequate for interpreting experimental results because they have low R^2 values.

Table 6 Study of intraparticle diffusion

Column size (cm)	qe / C	K1/ K2/Kdif.	R^2
6	2.513	-0.0063	0.9401
8	5.752	-0.0426	0.9532
10	6.935	-0.0137	0.9657

3.5. Regeneration study of adsorbent

Adsorption capabilities are impacted by the frequency of adsorbent recycling After three cycles, their respective adsorption capacities are shown to be 21.56 mg/L, which is an 82.36%, 84.17%, and 88.62% reduction from their initial adsorption capacities (Teutli-Sequeira *et al.*, 2013). The discoveries established that the adsorbent has strong cyclic adsorption presentation with a straightforward departure

characteristic following adsorption as a result of its superior magnetic characteristics, which may more competently happen the action necessities.

4. Conclusion

Azo dye from textile effluent was analysed together with its adsorption onto biochar produced from Annona reticulata. as well as the volatilization of chitosan molecules for efficient adsorption in packed bed columns and dye adsorption breakthrough data. The effects of bed height, flow velocity, and initial dye attentiveness with packed bed adsorption were examined along with the possibility of column regeneration and reuse. The parameters such as cradle volume, amount transmission region, bed consumption, and adsorbent convention were assessed using the break through curves. For all operating circumstances, the length of the unoccupied bed was shorter than the adsorption column, which grows as the mass transfer zone expands. Three different sized columns were utilized to explore Annona reticulata's ideal bed height. Hence, the adsorption capacity for a 6 cm column was 67.18%, an 8 cm column was 75.88%, and a 10 cm column was 94.37%. The adsorption models like the Bed Depth Service Thomas model and the Adam-Boharts models have been used to analyze the columns distinctive design characteristics. Using the origin software, the model's parameters have been determined. With R^2 0.975, Thomas and Adam-Boharts models were determined to be the best adsorption models out of four to examine column performance. Adam-boharts and Thomas models' average errors were calculated to be 0.0154 and 0.0263, respectively. According to the findings, the adsorption capacity in a 10 cm column is higher under optimal conditions, with a range of 94.37%. The column efficiency as measured by bed capacity up to the breaking point, the mass transfer zone, and bed utilization also demonstrates a significant improvement in the adsorptions process. SEM, XRD, and FTIR were used to analyze the surface properties of biochar made from Annona reticulata and volatilized by chitosan. In the mean of azo dye removal, the intra particle diffusion indicated the linear connection with adsorbent. The regeneration capacity was established, and it demonstrated that the adsorbent functions effectively over three study cycles.

Conflict of Interest

The authors declare no conflict of interest.

Acknowledgement

The authors extend their appreciation to the Researchers Supporting Project number (RSPD2023R667), King Saud University, Riyadh, Saudi Arabia.

References

Al-Amrani W.A., Lim P.E., Seng C.E and Ngah W.S.W. (2014). Factors affecting bio-decolorization of azo dyes and COD removal in anoxic–aerobic REACT operated sequencing batch reactor, *Journal of the Taiwan institute of chemical engineers*, **45**, 609–616.

Amani-Ghadim A.R., Aber S., Olad A and Ashassi-Sorkhabi H. (2013). Optimization of electrocoagulation process for removal of an azo dye using response surface methodology and investigation on the occurrence of destructive side reactions, Chemical engineering processing: *Process Intensification*, **64**, 68–78.

DadbanShahamat Y., Masihpour M., Borghei P. and Rahmati S.H. (2022). Removal of azo red-60 dye by advanced oxidation process O3/UV from textile wastewaters using Box-Behnken design, *Inorganic chemistry communications*, **143**, 109785.

Gao H., Zhao S., Cheng X., Wang X., Zheng L. (2013). Removal of anionic azo dyes from aqueous solution using magnetic polymer multi-wall carbon nanotube nanocomposite as adsorbent, *Chemical engineering journal*, **223**, 84–90.

Gnanasekaran L., Chen W.H. and Soto-Moscoso M. (2022). Highly operative NiO/ZnO nanocomposites for photocatalytic removal of azo dye, *Chemosphere*, **308**, 136528.

Gokulan R., Prabhu G.G. and Jegan J. (2019). Remediation of complex remazol effluent using biochar derived from green seaweed biomass, *International Journal of Phytoremediation*, **21**(12), 1179–1189.

Gokulan R. and Mohan Kumar N. (2014). Optimization of Conditions for Bio hydrogen Production from Industrial Waste by Anaerobic Co-digestion, *Nature Environment and Pollution Technology*, **13**(04), 791–794.

Gokulan R., Avinash A., Prabhu G.G. and Jegan J. (2019). Remediation of remazol dyes by biochar derived from Caulerpa Scalpelliformis - An eco-friendly approach, *Journal of Environmental Chemical Engineering*, **7** (5), 103297.

Gokulan R., Balaji S. and Sivaprakasam P. (2021). Optimization of Remazol Black B Removal Using Biochar Produced from Caulerpa scalpelliformis Using Response Surface Methodology, *Advance in Materials sciences and Engineering*.

Gokulan R., Kalyani G. and Killi S. (2022). Experimental Investigation on Reactive Orange 16 Removal Using Waste Biomass of Ulva prolifera, *Advances in material sciences and engineering*, Article ID 2689385.

Gokulan R., Kalyani G. and Killi S. (2022). Removal of Reactive Red 120 in a Batch Technique Using Seaweed-Based Biochar: A Response Surface Methodology Approach, *Journal of Nanomaterials*, Hindawi Publications, Article ID 7604383.

Gokulan R., Kavipriya S., Krishnakumar S., Dineshkumar R., Krishnapriya S. and Pradeepa Sri G. (2022). Extraction of biodiesel from wastewater using microalgae Chlorella Vulgaris, *Global NEST Journal*.

Gokulan R., Prabhu G.G. and Jegan J. (2019). A novel sorbent Ulva lactuca-derived biochar for remediation Remazol brilliant orange 3R in packed column, *Water Environment Research*, **91** (7), 642–649.

Gokulan R., Prabhu G.G., Avinash A. and Jegan J. (2020). Experimental and Chemometric analysis of bioremediation of remazol dyes using biochar derived from green seaweeds, *Desalination and Water Treatment*, **184**, 340–353.

Gokulan R., Prabhu G.G., Murugadoss J.R. and Hariharasuthan S. (2018). Optimization of bio-hydrogen production from bio-wastes", Ecology, *Environment and Conservation*, **24**(1), 284–287.

Gokulan R., Pradeepkumar S and Elias G. (2021). Continuous Sorption of Remazol Brilliant Orange 3R Using Caulerpa scalpelliformis Biochar, *Advances in Materials Science and Engineering*, Article ID 6397137, 7.

Gokulan R., Praveen S., Avinash A. and Saravanan S. (2021). Soft computing-based models and decolorization of Reactive Yellow 81 using Ulva Prolifera biochar, *Chemosphere*, **287**, Part 4, Jan (2022), 132368.

Gokulan R., Sathish N. and Praveen Kumar R. (2013). Treatment of Grey Water Using Hydrocarbon Producing Botryococcus braunii, *International Journal of Chemtech Research*, **05**(03), 1390–1392.

Gokulan R., Vijayakumar A., Rajesh Kumar V. and Praveen S. (2020). Remazol Effluent Treatment in Batch and Packed Bed Column Using Biochar Derived from Marine Seaweeds, Nature, *Environment and Pollution Technology*, **19**, 1931–1936.

Gopala Krishna G.V.T., Sivasankar V. and Senthil Kumar M. (2015). Coagulation performance evaluation of natural and synthetic coagulants in waste water treatment, *ARPN Journal of Engineering and Applied Sciences*, **10**, 6.

Gungor O., Yilmaz A., Memon S. and Yilmaz M. (2008). Evaluation of the performance of calix arene derivatives as liquid phase extraction material for the removal of azo dyes, *Journal of hazardous materials*, **158**, 202–207.

Hariharan T., Gokulan R., Saravanan R V. and Rahman D.Z. (2022). Batch and Packed Bed Column Studies of Azo Dyes Adsorption from the Aqueous Solutions Using Activated Sugarcane Bagasse Charcoal Adsorbent: Isotherm and Kinetic Studies, *Global NEST Journal*.

Haris M., Khan M.W., PazFerreiro J., Mahmood N. and Eshtiagi N. (2022). Synthesis of functional hydrochar from olive waste for simultaneous removal of azo and non-azo dyes from water, *Chemical engineering journal advances*, **9**, 100233.

Hashemi S.H. and Kaykhaii M. (2022). Chapter 15 - Azo dyes: Sources, occurrence, toxicity, sampling, analysis, and their removal methods, *Emerging fresh water pollutants*, **20**, 267–287.

Hua L., Ma H. and Zhang L. (2013). Degradation process analysis of the azo dyes by catalytic wet air oxidation with catalyst CuO/γ-Al2O3., *Chemosphere*, **90**, 143–149.

Ilavarasan N., Rao Y.S., Gokulan R. and Aravindan A. (2022). Investigation of Copper Ion adsorption using Activated Sawdust Powder: Isotherm, Kinetic and Thermodynamic studies, *Global NEST Journal*.

Jankowska K., Su Z., Zdarta J., Jesionowski T. and Pinelo M. (2022). Synergistic action of laccase treatment and membrane filtration during removal of azo dyes in an enzymatic membrane reactor upgraded with electrospun fibers, *Journal of hazardous materials*, **435**, 129071.

Jegan J., Praveen S., Muthu Kumar B., Pushpa T.B. and Gokulan R. (2021). Box–Behnken experimental design for the optimization of Basic Violet 03 dye removal by groundnut shell derived biochar, *Desalination and Water Treatment*., **209**, 379–391.

Jegan J., Praveen S., Pushpa T.B. and Gokulan R. (2020). Biodecolorization of Basic Violet 3 using biochar derived from agricultural waste: Isotherm and Kinetics, *Journal of Bio based materials and Bioenergy*, **14**(3), 316–326.

Jegan J., Praveen S., Pushpa T.B. and Gokulan R. (2020). Evaluation of the adsorption capacity of Cocos Nucifera shell derived biochar for basic dyes sequestration from aqueous solution, *Energy Sources, Part A: Recovery, Utilization, and Environmental Effects*.

Jegan J., Praveen S., Pushpa T.B and Gokulan R. (2020). Sorption kinetics and isotherm studies of cationic dyes by arachis hypogaea shell derived biochar as low-cost adsorbent, *Applied Ecology and Environmental Research*, **18** (1), 1925–1939.

Kalyani G., Gokulan R. and Sujatha S. (2021). Biosorption of zinc metal ion in aqueous solution using biowaste of Pithophora cleveana wittrock and Mimusops elengi, *Desalination and Water Treatment*. **218**, 363–371.

Kalyani G., Mahendran S.P. and Gokulan R. (2020). Removal of lead metal ion using biowaste of Pithophora cleveana wittrock and Mimusops elengi, Energy Source Part A: Recovery, *Utilization and Environmental Effects*.

Kamboh M.A., Bhatti A.A., Solangi I.B., Sherazi S.T.H. and Memon S. (2014). Adsorption of direct black-38 azo dye on p-tert-butylcalix[6]arene immobilized material, *Arabian Journal of chemistry*, **7**, 125–131.

Krishnakumar B., Imae T., Miras J., Esquena J. (2014). Synthesis and azo dye photodegradation activity of ZrS2–ZnO nano-composites, *Separation and purification Technology*, **132**, 281–288.

Kumar M., Sujatha S., Gokulan R., Vijayakumar A., Praveen S. and Elayaraja S. (2021). Prediction of RSM and ANN in the remediation of Remazol Brilliant Orange 3R using biochar derived from Ulva Lactuca, *Desalination and Water Treatment*, **211**, 304–318.

Lach C.E., PauliC.S., Coan A.S., Simionatto E.L. and Koslowski L.A.D. (2022). Investigating the process of electrocoagulation in the removal of azo dye from synthetic textile effluents and the effects of acute toxicity on Daphnia magna test organisms, *Journal of water process engineering*, **45**, 102485.

Lenin Sundar M., Kalyani G., Gokulan R., Ragunath S. and Joga Rao H. (2021). Comparative adsorptive removal of Reactive Red 120 using RSM and ANFIS models in batch and packed bed column, Biomass Conversion and Biorefinery.

Li T., Yang X.L, Song H.L., Xu H. and Chen Q.L. (2022). Quinones contained in wastewater as redox mediators for the synergistic removal of azo dye in microbial fuel cells, *Journal of engineering management*, **301**, 113924.

Madhu K., Ravindiran G., Sivarethinamohan S., Pathanjali S.P.S., Saravanan P., Sellappan E. (2021). Biodecolorization of Reactive Red 120 in batch and packed bed column using biochar derived from Ulva reticulata, *Biomass Conversion and Biorefinery*.

Mahendran S., Gokulan R., Aravindan A., Rao H.J., Kalyani G., Praveen S., Pushpa T.B. and Senthil Kumar M. (2021). Production of Ulva prolifera derived biochar and evaluation of adsorptive removal of Reactive Red 120: batch, isotherm, kinetic, thermodynamic and regeneration studies, *Biomass Conversion and Biorefinery*.

Moradi O., Pudineh A. and Sedaghat S. (2022). Synthesis and characterization Agar/GO/ZnO NPs nanocomposite for removal of methylene blue and methyl orange as azo dyes from food industrial effluents, *Food and chemical toxicology*, **169**, 113412.

Morshedi D., Mohammadi Z., AkbarBoojar M. and Aliakbari F. (2013). Using protein nanofibrils to remove azo dyes from aqueous solution by the coagulation process, Colloids and surfaces B: *Biointerfaces*, **112**, 245–254.

Murali V., Ong S.A., Ho L.N. and Wong Y.S. (2013). Evaluation of integrated anaerobic–aerobic biofilm reactor for degradation of azo dye methyl orange, *Bioresource technology*, **143**, 104–111.

Murugadoss J.R., Kalyani G., Gokulan R., Sivaprakasam P., Prabu M., Aravindan A., Praveen S. and Senthil Kumar M. (2021). Biochar from waste biomass as a biocatalyst for biodiesel production: an overview, Applied Nanoscience.

Ozdemir S., Cirik K., Akman D., Sahinkaya E. and Cinar O. (2013). Treatment of azo dye-containing synthetic textile dye effluent using sulfidogenic anaerobic baffled reactor, *Bioresource Technology*, **146**, 135–143.

Patel Y.N. and Patel M.P. (2013). Adsorption of azo dyes from water by new poly (3-acrylamidopropyl)-trimethylammoniumchloride-co-N, N-dimethylacrylamide superabsorbent hydrogel—Equilibrium and kinetic studies, *Journal of environmental chemical engineering*, **01**, 1368–1374.

Praveen S., Gokulan R., Jegan J. and Pushpa T.B. (2021). Techno-economic feasibility of biochar as biosorbent for basic dye sequestration, *Journal of Indian Chemical Society*.

Praveen S., Jegan J., Pushpa T.B. and Gokulan R. (2021). Artificial Neural Network Modelling for Biodecolorization of Basic Violet 03 from aqueous solution by biochar derived from agro-bio waste of groundnut hull: Kinetics and Thermodynamics, *Chemosphere*, Article ID.130191.

Praveen S., Jegan J., Pushpa T.B. and Gokulan R. (2021). Evaluation of the adsorptive removal of cationic dyes by greening biochar derived from agricultural bio-waste of rice husk, *Biomass Conversion and Biorefinery*.

Praveen S., Jegan J., Pushpa T.B., Gokulan R. and Bulgariu L. (2022). Biochar for removal of dyes in contaminated *water: an overview, Biochar*, **4**, Article ID: 10, 1–16.

Priya A.K., Gokulan R., Vijay Kumar A. and Praveen S. (2020). Biodecolorization of remazol dyes using biochar derived from Ulva reticulata: Isotherm, Kinetics, Desorption and Thermodynamic Studies, *Desalination and Water Treatment*, **200**, 286–295.

Pushpa T.B., Josephraj J., Saravanan P. and Ravindran G. (2019). Biodecolorization of Basic Blue 41 using EM based Composts: Isotherm and Kinetics, Chemistry select, **4**(34), 10006–10012.

Pushpa T.B., Praveen S., Gokulan R. and Jegan J. (2021). Continuous sorption of methylene blue dye from aqueous solution using effective microorganisms-based water hyacinth waste compost in a packed column, *Biomass Conversion and Biorefinery*.

Ragunath S., Atchyuth B.A.S., Rao G.S. and Gokulan R. (2022). Biodecolorization of Remazol Black B using Biochar produced from Coconut Shell: Batch, Desorption, Isotherm and Kinetic Studies, *Global NEST Journal*.

Rajeshkumar V., Senthil Kumar M., Al-Zaqri N. and Boshaala A. (2023). Adsorption of cationic dye (Red 95) from aqueous solution by biosynthesized nano particle of cumnium cyminum, *Global Nest Journal*, **25**, 1–10.

Rao H.J., Gokulan R., Ragunath S. and Praveen S. (2021). Optimization of process conditions using RSM and ANFIS for the removal of Remazol Brilliant Orange 3R in a packed bed column, *Journal of Indian Chemical Society*.

Ravindiran G. (2014). Best dilution ratio and GCMS analysis for the removal of nutrient from municipal wastewater by microalgae, *International Journal of Chemtech Research*, **06**(01), 663–672.

Ravindiran G. and Ragunath S. (2014). Comparative study on treatment of municipal wastewater with carbon dioxide sequestration by microalgae, *International Journal of ChemTech Research*, **06** (01), 609–618.

Ravindiran G., Elayaraja S., Navaneethan P., Rajeshkannan R. and Abinaya S. (2014). Assessment of physicochemical characteristics of municipal wastewater by microalgae, *International Journal of ChemTech Research*, **06**(01), 515–520.

Ravindiran G., Ganapathy G.P., Josephraj J. and Alagumalai A. (2019). A Critical Insight into Biomass Derived Biosorbent for Bioremediation of Dyes, Chemistry select, **4**(34), 9762–9775.

Ravindiran G., Jeyaraju R.M., Josephraj J. and Alagumalai A. (2019). Comparative Desorption Studies on Remediation of Remazol Dyes Using Biochar (Sorbent) Derived from Green Marine Seaweeds, Chemistry Select, **4**(25), 7437–7445.

Saravanan V.R., Yuvaraja R., Andal L. and Gokulan R. (2022). Batch, thermodynamic, and regeneration studies of Reactive Blue 19 using Ulva reticulata (biochar), *Desalination and Water Treatment*, **267**, 231–239.

Sathees Kumar V., Gokulan R., Geetha M.B. and Rahman D.Z. (2022). Biosorption of heavy metal ions from the aqueous solutions using groundnut shell activated carbon: batch adsorption, kinetic and thermodynamic studies, *Global NEST Journal*.

Senthil Kumar M., Kalyani G., Mahendran S., Joga Rao H., Gokulan R., Someswaran R., Latha C.J. and Palpandian M. (2021). Treatment of RO rejects wastewater by integrated coagulation cum adsorption process", *Polish Journal of Environmental Studies*, **30**, 5, 1–8.

Senthil Kumar M., Sivasankar V. and Gopalakrishna GVT. (2017). Quantification of benzene in groundwater sources and risk analysis in a popular South Indian Pilgrimage City–a GIS based approach, *Arabian Journal of Chemistry*, **10**, S2523–S2533.

Shirzad-Siboni M., Khataee A. and Joo S.W. (2014). Kinetics and equilibrium studies of removal of an azo dye from aqueous solution by adsorption onto scallop, *Journal of industrial and engineering chemistry*, **20**, 610–615.

Sujatha S., Gokulan R., Rahman Z. and Yogeshwaran V. (2022). Investigation of Mechanism of Metal Ion Adsorption from Aqueous Solutions using Prosopis Julyflora Roots: Batch and Fixed Bed Column Studies, *Global NEST*, March (2022).

Sujatha S., Gokulan R., Rao H.J, Kalyani G., Praveen S., Senthil Kumar M. (2021). Effective removal of remazol brillinat orange 3R using a biocharderived from Ulva reticulata, Energy Source Part A: Recovery, *Utilization and Environmental Effects*.

Sujatha S., Rao H.J., Kalyani G., Gokulan R. and Avinash A. (2021). Toward sustainable biodiesel production by solar intensification of waste cooking oil and engine parameter assessment studies, *Science of The Total Environment*, **804**, Article ID.150236.

Teutli-Sequeira A., Martınez-Miranda V., Solache-Rios M. and Linares-Hernandez I. (2013). Aluminum and lanthanum effects in natural materials on the adsorption of fluoride ions, *Journal of fluoride chemistry*, **148**, 6–13.

Tuttolomondo M.V., Alvarez G.S., Desimone M.F. and Diaz L.E. (2014). Removal of azo dyes from water by sol–gel immobilized Pseudomonas sp., *Journal of environmental chemical engineering*, **2**, 131–136.

Vucurovic V.M., Razmovski R.N., Miljic U.D. and Puskas V.D. (2014). Removal of cationic and anionic azo dyes from

aqueous solutions by adsorption on maize stem tissue, *Journal of Taiwan institute of chemical engineers*, **45**, 1700–1708.

Wang Y.Z., Wang A.J., Wen-Zong Liu W.Z. and Sun Q. (2013). Enhanced azo dye removal through anode biofilm acclimation to toxicity in single-chamber biocatalyzed electrolysis system, *Bioresource technology*, **142**, 688–692.

Xi Y., Shen Y., Yang F., Yang G., Liu C., Zhang Z. and Zhu D. (2013). Removal of azo dye from aqueous solution by a new biosorbent prepared with Aspergillus nidulans cultured in tobacco wastewater, *Journal of Taiwan institute of chemical engineers*, **44**, 815–820.

Xu L., Li X., Ma J., Wen Y. and Liu W. (2014). Nano-MnOx on activated carbon prepared by hydrothermal process for fast and highly efficient degradation of azo dyes, *Applied catalysis* A: General, **485**, 91–98.

Zhang H., Lu H., Zhang S., Liu G., Li G., Zhou J. and Wang J. (2014). A novel modification of poly(ethylene terephthalate) fiber using anthraquinone-2-sulfonate for accelerating azo dyes and nitroaromatics removal, *Separation and purification technology*, **132**, 323–329.

Zubair M., Aziz H., Ihsanullah I., Ahmad M.A. and Al-Harthi M.A. (2022). Engineered biochar supported layered double hydroxide-cellulose nanocrystals composite-: Synthesis, characterization and azo dye removal performance, *Chemosphere*. **307**, 136054.